Twofold Rattling Mechanism of Ultralow Thermal Conductivity in Vacancy-Ordered Double Perovskite Cs_2SnI_6

Un-Gi Jong,[*,†] Yun-Sim Kim,[†] Chol-Hyok Ri,[†] Yun-Hyok Kye,[†] Chol-Jin Pak,[†] Stefaan Cottenier,[‡] and Chol-Jun Yu[*,†]

†*Chair of Computational Materials Design (CMD), Faculty of Materials Science, Kim Il Sung University, Pyongyang, PO Box 76, Democratic People's Republic of Korea*

‡*Department of Electromechanical, Systems and Metal Engineering & Center for Molecular Modeling (CMM), Ghent University, Technologiepark-Zwijnaarde 46, BE-9052 Gent, Belgium*

E-mail: ug.jong@ryongnamsan.edu.kp; cj.yu@ryongnamsan.edu.kp

Abstract

Vacancy-ordered double perovskite offers a promising outlet for lowering the lattice thermal conductivity of perovskite, but remains hitherto unexplored. Using first-principles calculations, we investigate the thermal properties of vacancy-ordered double perovskite Cs_2SnI_6, comparing with conventional perovskite $CsSnI_3$. Based on scrutiny of crystalline structures and lattice vibrations, we propose a twofold ratting mechanism induced by Cs atoms and isolated SnI_6 octahedral clusters in Cs_2SnI_6 being different from $CsSnI_3$ with only Cs atom rattler. Our calculations reveal that the twofold rattlers in Cs_2SnI_6 scatter the heat-carrying acoustic phonons coupled with low-lying optical modes and lower the phonon group velocity. Electron localization function analysis supports the twofold rattling mechanism in Cs_2SnI_6. We predict lattice thermal conductivity κ of Cs_2SnI_6 at the temperature range from 300 to 1000 K, finding an exceptionally ultralow κ of 0.11 W/m·K at 300 K and thus paving a way to find perovskite-based thermoelectrics with high-performance and low-cost.

Graphical TOC Entry

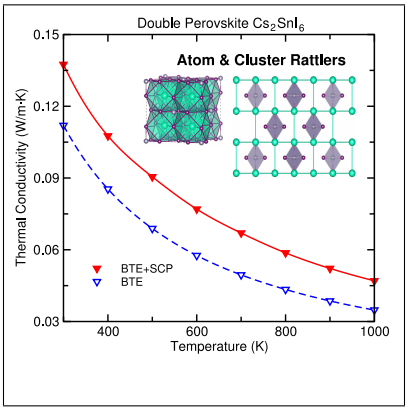

Highly efficient thermoelectric materials can innovate in manipulation and utilization of waste heat by turning it into electric power.[1–6] Besides for photovoltaic applications, halide perovskites with a chemical formula of ABX_3 (A: organic or inorganic monovalent cation, B: divalent metal cation, X: halide anion) have drawn increasing attention as a promising candidate for commercially viable thermoelectric materials.[7–13] With a simple and cost-effective synthesis, this is due to their ultralow thermal conductivities,[11–13] which ensure high figure of merit for thermoelectric performance defined as $ZT = S^2\sigma T/(\kappa_e + \kappa_l)$ (S: Seebeck coefficient, σ: electrical conductivity, κ: thermal conductivity by electron and lattice) and are related with extremely anharmonic lattice vibrations,[14–17] as well as the unique optoelectronic properties.[18–25] The organic-inorganic hybrid perovskite $CH_3NH_3PbI_3$, being prototype of halide perovskite for solar cells, was found to exhibit an ultralow thermal conductivity of 0.5 W/m·K at room temperature by experiment[13] or even 0.05 W/m·K by first-principles calculation,[15] being comparable with those of gases and much lower than those of solids. Based upon theoretical calculations, such ultralow κ was mainly ascribed to the rotational motion of the organic $CH_3NH_3^+$ cation.[26–28] For all-inorganic perovskites $CsPbI_3$ and $CsSnI_3$ in orthorhombic δ- or γ-phase, Yang and co-workers[12] also found ultralow κ below 0.45 W/m·K at room temperature. This raised the question of the former insight because the elemental Cs^+ cation could not follow the rotational modes like the molecular $CH_3NH_3^+$ cation. Therefore, metal-halide cluster rattling modes, being localized vibrational mode by collective motions of atoms, were suggested to be the main origin of the ultralow thermal conductivity in the all-inorganic halide perovskites.[12] Recently, Xie *et al.*[11] demonstrated a strong correlation between thermal conductivity and lattice dynamics in cubic $CsSnBr_{3-x}I_x$, which exhibits the ultralow κ of 0.32 W/m·K at 550 K. Based on the crystallographic data and theoretical calculations, they suggested the heavy Cs atoms as rattlers, inducing the strong coupling of the low frequency optical phonons with the heat carrying acoustic phonons. This resulted in the severe phonon resonance scattering, thereby producing the ultralow lattice thermal conductivity in the all-inorganic perovskites.[11]

Halide perovskites have a great diversity of crystalline structures,[29] providing a degree of free-

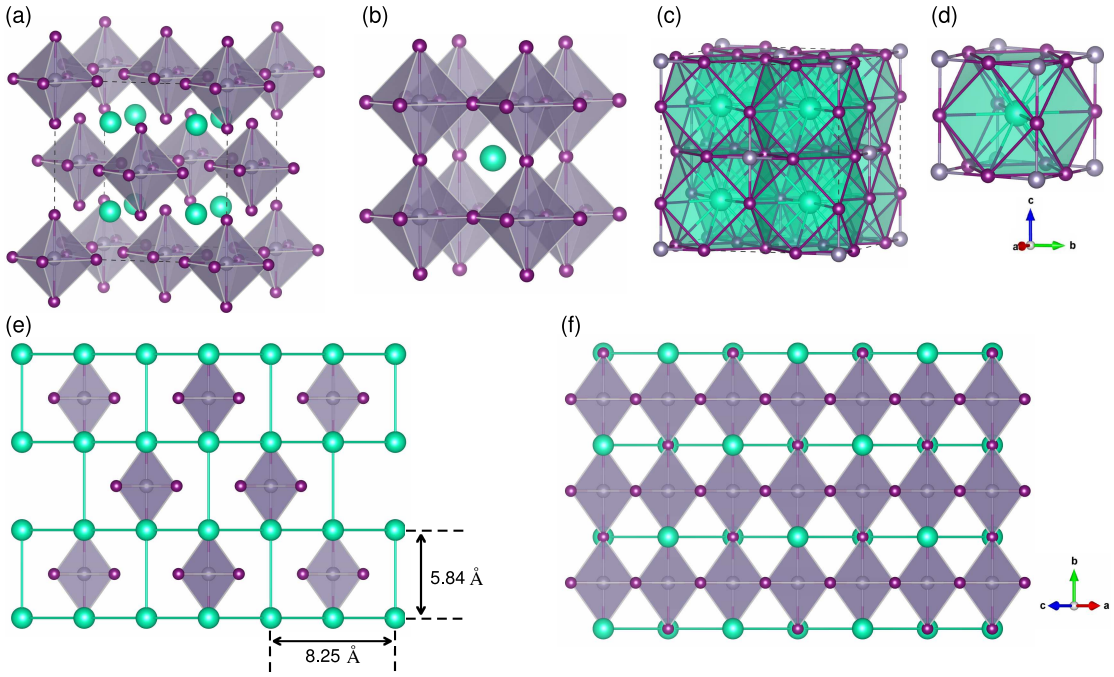

Figure 1: Crystalline structures of (a) vacancy-ordered double perovskite Cs_2SnI_6 with cubic $Fm\bar{3}m$ space group and (b) conventional perovskite $CsSnI_3$ with cubic $Pm\bar{3}m$ space group. Local coordination environments of Cs atom-rattler inside a cub-octahedral cage formed by I atoms for (c) Cs_2SnI_6 and (d) $CsSnI_3$. Illustrations of isolated and corner-sharing SnI_6 octahedra inside cage-like structures composed of Cs atoms for (e) Cs_2SnI_6 and (f) $CsSnI_3$. Green, gray and purple balls represent Cs, Pb and I atoms. Crystalline structures were visualized by using VESTA code.[34]

dom for further tuning the thermal conductivity. One example is the halide double perovskite $Cs_2AgBiBr_6$ that can be formed by replacing the divalent two Pb^{2+} cations with a pair of monovalent Ag^+ and trivalent Bi^{3+} cations. Using first-principles lattice dynamics, Klarbring *et al.*[30] demonstrated that this double perovskite can exhibit an ultralow κ as 0.33 W/m·K at room temperature even in high-symmetric cubic phase, being originated from the softness and anharmonicity in its phonon dispersion. Instead of such replacing, removing half of the divalent cations gives a vacancy-ordered double perovskite with a chemical formula of A_2BX_6,[17,31–33] which can further reduce κ by intensifying the lattice anharmonicity and enhancing the rattling vibrations. However, thermal transport properties of the vacancy-ordered double perovskites have yet been untouched in both experiment and simulation.

In this work, we first predict an ultralow thermal conductivity of vacancy-ordered lead-free double perovskite Cs_2SnI_6 in cubic phase by density functional theory (DFT) phonon calculations.

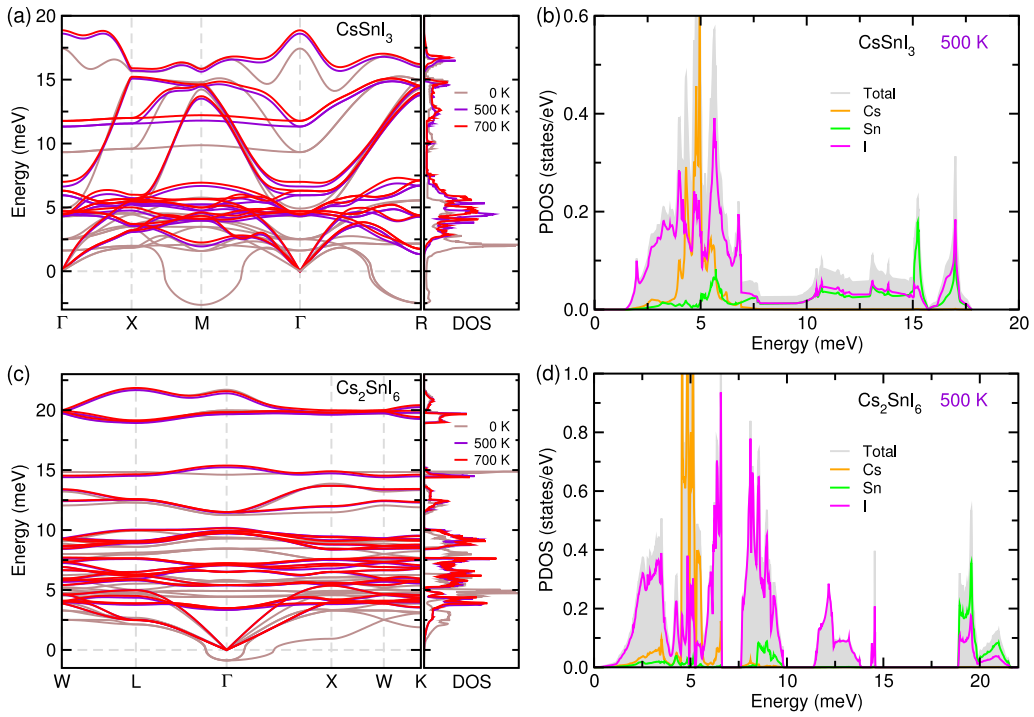

Figure 2: Phonon dispersion curves and total density of states (TDOS) at different temperatures of 0, 500 and 700 K for (a) $CsSnI_3$ and (c) Cs_2SnI_6. Atom-projected density of states (PDOS) at 500 K for (b) $CsSnI_3$ and (d) Cs_2SnI_6.

Twofold rattling mechanism is proposed for explaining the ultralow κ. We show highly anharmonic feature of its lattice dynamics at finite temperature, being different from that of conventional perovskite $CsSnI_3$. An exceptionally low κ of 0.11 W/m·K is obtained, being almost one sixth of $CsSnI_3$ at room temperature. We perform detailed analysis of lattice vibrations and electron localization function, revealing the key role of the twofold rattling vibrations induced by both Cs atoms and SnI_6 octahedral clusters in scattering the heat-carrying acoustic phonons and thus reducing the thermal conductivity of Cs_2SnI_6.

We start with a scrutiny into crystalline structure of the vacancy-ordered double perovskite Cs_2SnI_6 in cubic phase with space group $Fm\bar{3}m$,[35] comparing to cubic $CsSnI_3$ with space group $Pm\bar{3}m$.[36] As shown in Figure 1(a) and (b), replacing every other Sn atom with a vacancy in $CsSnI_3$ leads to the vacancy-ordered double perovskite Cs_2SnI_6.[37–39] The crystal structure of Cs_2SnI_6 can be regarded as a defect variant of $CsSnI_3$ with isolated SnI_6 octahedra bridged by Cs atoms, which is in a striking contrast to corner-sharing arrangement of octahedra in $CsSnI_3$.[17,32,33] In spite of

such structural change, the local coordination environments of Cs atoms do not alter distinctly, as they reside in the ideal 12-coordinated cub-octahedral geometry formed by I atoms (Figure 1(c) and (d)). Only the Cs−I bond length is slightly contracted from 4.37 Å in $CsSnI_3$ to 4.13 Å in Cs_2SnI_6. This is correlated with decreases of Sn−I bond length and lattice constant caused by the ordered Sn vacancies in Cs_2SnI_6. Note that the Cs−I distance of 4.13 Å in Cs_2SnI_6 is still longer than that of 3.92 Å in cubic CsI crystalline solid and the sum of ionic radii of Cs^+ and I^- (3.87 Å). Therefore, it is clear that in Cs_2SnI_6 a Cs atom is located inside the over-sized cub-octahedral cage, expecting its role as a heavy rattler that can drive the lattice anharmonicity as in $CsSnI_3$.

Meanwhile, the local environment of SnI_6 octahedra is significantly changed. In the case of vacancy-ordered double perovskite Cs_2SnI_6, they are isolated and located inside the over-sized cage-like structures composed of the Cs atoms. This is contrary to the corner-sharing arrangement of SnI_6 octahedra in $CsSnI_3$, as shown in Figure 1(e) and (f). Owing to the sufficient interstitial space in the cage-like structures, the isolated octahedra in Cs_2SnI_6 are loosely bound to their neighbors, so that they can play a similar role to the Cs atom rattlers. However, the corner-sharing octahedra in $CsSnI_3$ are tightly connected with each other, thereby implying impossibility for them to act as rattlers. From this consideration on their crystalline structures, we can suppose both the Cs atoms and the isolated SnI_6 octahedra to be rattlers, indicating twofold rattling motions in Cs_2SnI_6. When compared to $CsSnI_3$ with only Cs atom rattler, the lattice anharmonicity can be further enhanced, possibly reducing κ in Cs_2SnI_6.

In order to verify this hypothesis of twofold rattling mechanism, we then perform lattice dynamics calculations for Cs_2SnI_6 and $CsSnI_3$ using supercells to obtain their phonon energies and density of states (DOS) (see Supporting Information for computational details). Figure 2(a) and (c) show the phonon dispersion curves and total DOS calculated at 0 K for $CsSnI_3$ and Cs_2SnI_6, respectively (see Figure S1 for convergence test of phonon dispersion curves according to supercell size). Note that the phonon dispersion curves obtained in this work are in good agreement with the previous calculations obtained by different methods.[17,40] For $CsSnI_3$, the soft phonon modes with the imaginary phonon energies are identified at M and R points of the Brillouin zone (BZ).

This is agreed with the recent experimental finding that $CsSnI_3$ can be stabilized in cubic phase only at high temperature over 441 K, and transformed to tetragonal $P4/mbm$ at 362 K[41] and to orthorhombic $Pnma$[42] phases at room temperature.[11] The soft phonon modes are also found at Γ point for Cs_2SnI_6, which is at odds with the experimental observation that Cs_2SnI_6 can adopt the cubic structure at the whole range of temperature.[37,38] As Xie *et al.*[11] already pointed out that the major reason for the anharmonic phonon modes in cubic $CsSnI_3$ is the Cs atom rattlers, moving away from the center of the cub-octahedral cage due to the local distortion of SnI_6 octahedra, the anharmonic phonon modes presented even in the dynamically stable cubic Cs_2SnI_6 are associated with the rattlers. That is, they are just caused by the twofold rattling vibrations of the Cs atom and octahedral cluster, as expected above.

In the previous work,[17] we have calculated the potential energy surface (PES) of cubic Cs_2SnI_6 following the phonon eigenvectors corresponding to the anharmonic modes at the BZ center. The double perovskite Cs_2SnI_6 exhibits very flat landscape for PES with the low energy barrier below 11 meV per formula unit for structural transition from cubic to symmetry-broken local phases.[17] This energy barrier is much lower than the thermal energy k_BT at room temperature (~26 meV) and that for $CsSnI_3$ (~40 meV).[11] This indicates that Cs_2SnI_6 is not only dynamic, fluctuating between the symmetry-lowered local structures and just appearing cubic phase on average, but also highly anharmonic.[17] Such analysis is consistent with the recent work for another double perovskite $Cs_2AgBiBr_6$,[30] emphasizing that its lattice dynamics in cubic phase is strongly anharmonic and the phase transition is quite different from that of the conventional perovskite. On the other hand, the emergence of such imaginary phonon modes requires anharmonic phonon renormalization (APRN) at finite temperature.[43,44]

To this end, we perform self-consistent phonon (SCP) calculations to consider the anharmonic effects when elevating temperature. Here, the anharmonic phonon eigenvalues as a function of temperature can be computed from the pole of the Green's function beyond perturbation theory, as implemented in the ALAMODE code.[45,46] Figure 2(a) and (c) show the obtained anharmonic phonon dispersion curves at finite temperatures of 500 and 700 K for $CsSnI_3$ and Cs_2SnI_6, re-

spectively (see Figure S3 and S4 for the anharmonic phonon dispersion curves at the temperature range from 300 to 1000 K for Cs_2SnI_6 and $CsSnI_3$, respectively). When compared with the harmonic phonon dispersions at 0 K, the imaginary phonon eigenvalues were found to become real by renormalization, demonstrating that the cubic phases for both $CsSnI_3$ and Cs_2SnI_6 become dynamically stable at high temperature. As going from 0 K to finite temperature, both the acoustic and optical modes for $CsSnI_3$ are distinctly changed in the whole range of phonon frequency by APRN, whereas the change was not radical for Cs_2SnI_6. This also indicates the thermal instability of cubic $CsSnI_3$ at 0 K while relatively high stability of Cs_2SnI_6. Importantly, the acoustic modes of Cs_2SnI_6 are getting flattened going from the BZ center to the BZ boundary around 5 meV of phonon energy in contrast with those of $CsSnI_3$ that are still quite dispersive. Together with the strong coupling with the optical modes, this gives an evidence of stronger lattice anharmonicity in Cs_2SnI_6. Moreover, nearly flat optical modes with the lowest energy of ~3.8 meV at Γ-point appear in the acoustic region for Cs_2SnI_6. Meanwhile, all the optical modes of $CsSnI_3$ look more dispersive along arbitrary direction in the BZ. It is widely accepted that such flat optical modes are responsible for slow group velocity v_g and act as strong scattering centers for low-lying acoustic modes. Based on such consideration, we can conceive that Cs_2SnI_6 exhibits much slower v_g and shorter lifetime of phonon than $CsSnI_3$.

To further understand the difference in lattice vibration between $CsSnI_3$ and Cs_2SnI_6, we plot their atom-projected phonon DOS (PDOS) calculated from the SCP calculations at 500 K in Figure 2(b) and (d). Both the perovskites are found to have the low-lying optical phonon modes around ~5meV, which are mostly associated with the rattling vibrations of Cs atoms. The Cs-related PDOS in Cs_2SnI_6 looks narrower than in $CsSnI_3$, verifying its stronger rattling vibrations of Cs atoms. Moreover, we observe separate peaks around 2.5, 5.0, 6.3 and 8.5 meV in the acoustic and low-lying optical regions for Cs_2SnI_6, which are mainly ascribed to the vibrations of I atoms with small contributions of Sn atoms. By contrast, united peak is seen in the region between 3 and 7 meV for $CsSnI_3$. These additional separate peaks in Cs_2SnI_6 can be regarded as the evidence of rattling vibrations of SnI_6 octahedral clusters, *i.e.*, collective motions of Sn and I atoms as shown

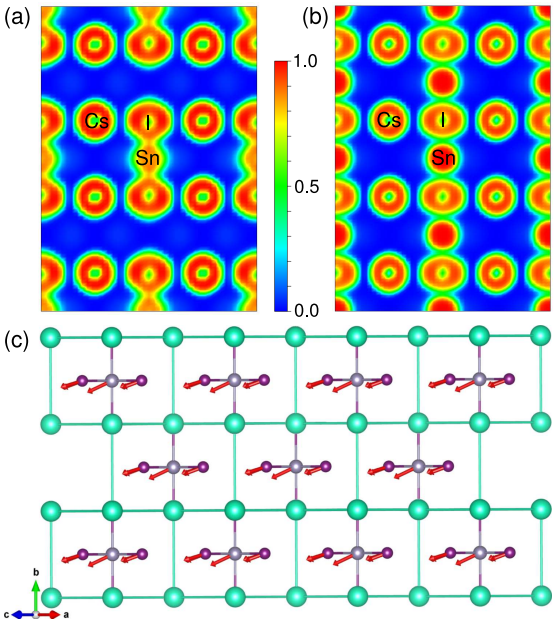

Figure 3: Electron localization function in (110) plane of (a) Cs_2SnI_6 and (b) $CsSnI_3$. (c) Collective motion of Sn and I atoms in the host cage of Cs atoms, according to the phonon eigenvectors of low-lying optical modes in Cs_2SnI_6.

in Figure 3(c). Note that through such strong rattling vibrations, guest atoms or clusters swing in the host cage structures, scattering the heat-carrying phonons.[11,47,48]

We analyze the electron localization functions (ELFs) of Cs_2SnI_6 and $CsSnI_3$ in Figure 3(a) and (b), which help find electronic mechanism of the anharmonic rattling modes. As the ELF value increases, the electrons are considered to be more localized and thus the atomic bonding to be transformed into the covalent type. In the ELF pictures, we can see almost perfect spheres around Cs atoms but different features around Sn and I atoms for the two perovskites. Obviously there is more charge sharing between Sn and I atoms in Cs_2SnI_6 than in $CsSnI_3$, which is associated with the bond length contraction in the double perovskite. Moreover, no charge is observed between the neighboring octahedra due to the vacancies in Cs_2SnI_6 in contrast with $CsSnI_3$. This implies that the SnI_6 octahedral clusters in Cs_2SnI_6 are loosely bound to the neighbors, causing the cluster-rattling vibrations. In addition, non-spherical ELF around Sn and I atoms in Cs_2SnI_6, reflecting the inhomogeneous connectivity of constituent atoms, explains the electronic origin of phonon anharmonicity.[48] Summing up discussions so far, there exist the octahedral cluster rattlers as well as the

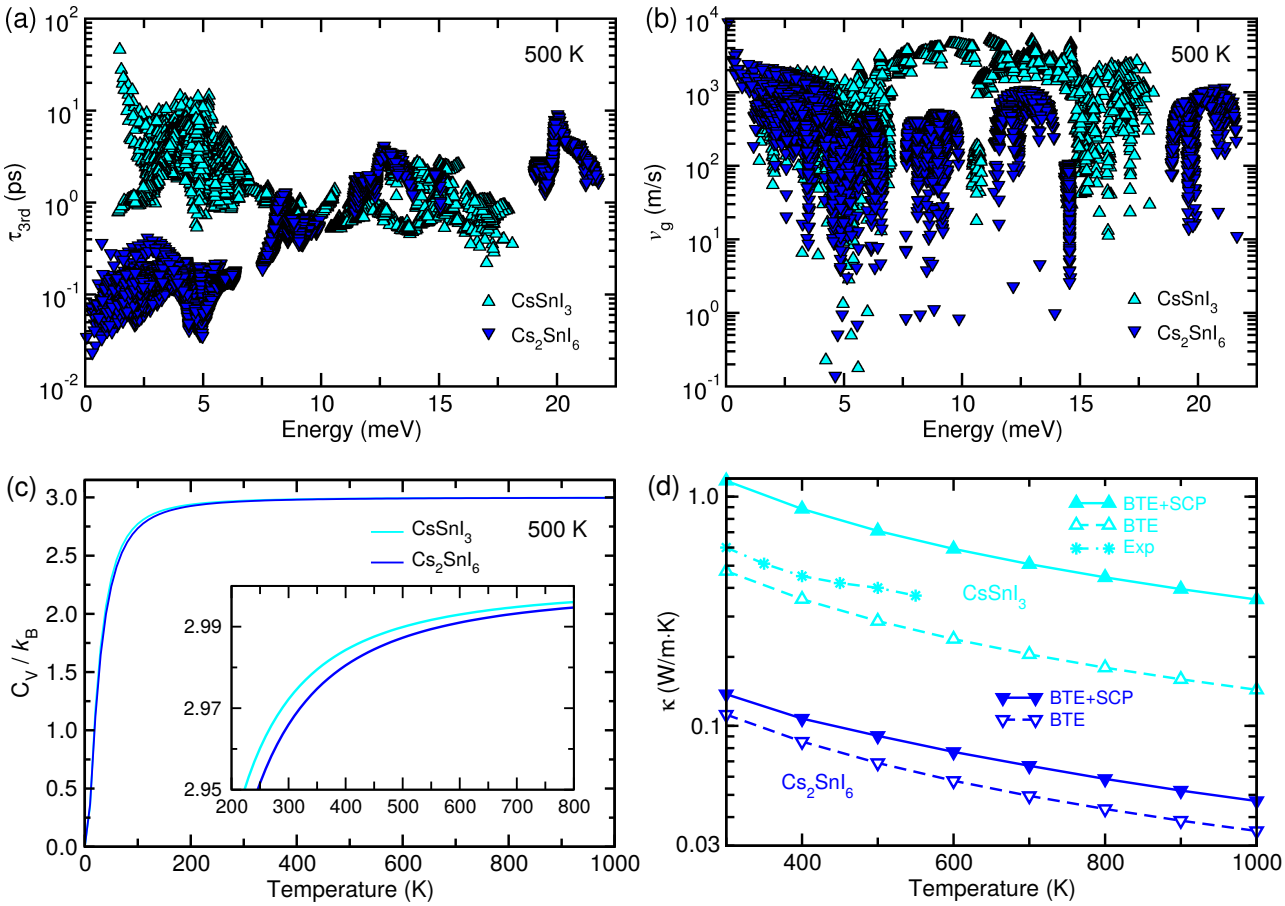

Figure 4: Phonon lifetime τ_{3rd} (a), phonon group velocity v_g (b), heat capacity C_V (c) computed by SCP theory at 500 K, and temperature-dependent κ by harmonic and SCP calculations with experimental results[11] (d), respectively for Cs_2SnI_6 and $CsSnI_3$.

Cs atom-rattlers in Cs_2SnI_6, whereas only the Cs atom rattlers exist in $CsSnI_3$. Accordingly, it can be surely expected that the thermal conductivity of vacancy-ordered double perovskite Cs_2SnI_6 is significantly lower than the conventional perovskite $CsSnI_3$.

Finally, we calculate the lattice thermal conductivities of Cs_2SnI_6 and $CsSnI_3$ by solving the Boltzmann transport equation (BTE) within perturbation theory combined with solution of SCP equation. Figure 4(a) and (b) show the phonon lifetime τ_{3rd} and phonon group velocity v_g as functions of phonon energy, calculated from SCP solution at 500 K considering the three-phonon scattering (see Figure S5 and S6 for cumulative κ, and average τ_{3rd} and v_g, respectively). When compared with $CsSnI_3$, τ_{3rd} in Cs_2SnI_6 is found to decrease more rapidly as decreasing phonon energy below 7.5 meV, which is ascribed to the aforementioned twofold rattling vibrations of Cs

atoms and the octahedral clusters. Moreover, v_g in Cs_2SnI_6 is observed to be smaller in the whole range of phonon energy, possibly due to the flattened phonon dispersion of Cs_2SnI_6. As shown in Figure 4(c), Cs_2SnI_6 has smaller heat capacity C_V than $CsSnI_3$ at the whole range of temperature because of lack in Sn−I bonds by the Sn vacancies. Having the necessary quantities of τ, v_g and C_V, we assess κ of Cs_2SnI_6 and $CsSnI_3$ as functions of temperature, as shown in Figure 4(d) (see Figure S2 for convergence test of κ according to the size of q-point mesh). When employing the SCP energies for solving BTE (BTE + SCP), κ is observed to be larger than that calculated with harmonic phonon energies (BTE), as has been found out in the previous works.[30,45,46] For the case of $CsSnI_3$, the calculated values of κ with BTE and BTE + SCP are slightly smaller and larger than the experimental values,[11] indicating a reasonable accuracy of our calculations. As expected from the smaller values of τ, v_g and C_V, the lattice thermal conductivity κ of Cs_2SnI_6 is about a sixth lower than that of $CsSnI_3$ in the temperature range of interest. At 300 K, κ of Cs_2SnI_6 is proved to be ultralow as 0.11 W/m·K with BTE + SCP, being a third of 0.33 W/m·K of the double perovskite $Cs_2AgBiBr_6$.[30] As has been found out,[49–51] solids in disordered complex structures and/or large unit cells tend to have low thermal conductivities, while the manifestation of ultralow thermal conductivity in an ordered high-symmetry cubic structure, such as that of Cs_2SnI_6, is unusual with the twofold rattling vibrations as the underlying mechanism.

In summary, we have performed first-principles calculations to investigate the thermal properties of vacancy-ordered double perovskite Cs_2SnI_6 while comparing with the conventional perovskite $CsSnI_3$. By scrutinizing the crystalline structures and analyzing the phonon dispersions, we have conceived that both the Cs atoms and the isolated SnI_6 octahedra in Cs_2SnI_6 act as rattlers, *i.e.*, twofold rattlers, unlike the $CsSnI_3$ with only Cs atom rattler. Our calculations have shown much shorter phonon lifetime and lower group velocity due to the strong scattering of heat-carrying acoustic phonons and flattened phonon dispersions in Cs_2SnI_6, revealing that the twofold rattling modes stimulate the lattice anharmonicity. We have estimated the lattice thermal conductivities of Cs_2SnI_6 and $CsSnI_3$ at the temperature range from 300 to 1000 K, finding an exceptionally low κ of 0.11 W/m·K at 300 K for Cs_2SnI_6. We believe that our work opens up new potential applications

of the vacancy-ordered double perovskite for high-performance and low-cost thermoelectrics.

Computational Methods

Density functional theory (DFT) calculations were performed by using the projector-augmented wave (PAW) method[52] as implemented in the Vienna Ab Initio Simulation Package (VASP).[53,54] Valence electron configurations of the atoms in the PAW functions are Cs–$5s^2 5p^6 6s^1$, Sn–$5s^2 5p^2$ and I–$5s^2 5p^5$. The exchange-correlation interactions between valence electrons was described with the PBEsol functional[55] within the generalized gradient approximation (GGA). Kinetic energy cutoff of 800 eV was used for a plane-wave basis set and a k-point mesh of (12×12×12) was for Brillouin zone (BZ) integration, guaranteeing the total energy accuracy within 3 meV per unit cell. The atomic positions were relaxed until the atomic forces converged to 10^{-3} eV/Å, while the energy convergence criterion was set to 10^{-8} eV.

To perform harmonic phonon calculations, we extracted harmonic interatomic force constants (IFCs) by utilizing the finite displacement method with 3×3×3 supercell, as implemented in the ALAMODE code.[45,46] The relevant atoms were displaced from their equilibrium positions by 0.01 Å considering the crystalline symmetry. We performed self-consistent phonon (SCP) calculations to consider anharmonic effects at finite temperature by calculating the anharmonic phonon eigenvalues as a function of temperature from the pole of the Green's function beyond perturbation theory. The anharmonic IFCs were obtained by performing the compressive sensing lattice dynamics (CSLD)[56] with over 60 configurations where all of the atoms were displaced randomly with large displacements. Using the calculated 3rd-order IFCs, we solved phonon Boltzmann transport equation (BTE) with a q-point mesh of (24×24×24) within the relaxation time approximation (RTA) to estimate the lattice thermal conductivity.

Associated Content

Supporting Information

The Supporting Information is available free of charge on the ACS Publications website at DOI: xxx/xxx.

Computational details, convergence test for harmonic phonon calculations using 2×2×2 and 3×3×3 supercells, lattice thermal conductivity of $CsSnI_3$ at different q-point meshes, anharmonic phonon dispersion curves, cumulative κ, and average τ_{3rd} and v_g at the temperature range from 300 to 1000 K for $CsSnI_3$ and Cs_2SnI_6 (PDF)

Author information

Corresponding Authors

Un-Gi Jong – Chair of Computational Materials Design (CMD), Faculty of Materials Science, Kim Il Sung University, Pyongyang, PO Box 76, Democratic Peoples' Republic of Korea; orcid.org/0000-0003-4654-2449; E-mail: ug.jong@ryongnamsan.edu.kp

Chol-Jun Yu – Chair of Computational Materials Design (CMD), Faculty of Materials Science, Kim Il Sung University, Pyongyang, PO Box 76, Democratic Peoples' Republic of Korea; orcid.org/0000-0001-9523-4325; E-mail: cj.yu@ryongnamsan.edu.kp

Authors

Yun-Sim Kim – Chair of Computational Materials Design (CMD), Faculty of Materials Science, Kim Il Sung University, Pyongyang, PO Box 76, Democratic Peoples' Republic of Korea

Chol-Hyok Ri – Chair of Computational Materials Design (CMD), Faculty of Materials Science, Kim Il Sung University, Pyongyang, PO Box 76, Democratic Peoples' Republic of Korea

Yun-Hyok Kye – Chair of Computational Materials Design (CMD), Faculty of Materials Science, Kim Il Sung University, Pyongyang, PO Box 76, Democratic Peoples' Republic of Korea

Chol-Jin Pak – Chair of Computational Materials Design (CMD), Faculty of Materials Science, Kim Il Sung University, Pyongyang, PO Box 76, Democratic Peoples' Republic of Korea

Stefaan Cottenier – Department of Electromechanical, Systems and Metal Engineering & Center for Molecular Modeling (CMM), Ghent University, Technologiepark-Zwijnaarde 46, BE-9052 Gent, Belgium; orcid.org/0000-0003-2541-8043

Notes

The authors declare no competing financial interest.

Acknowledgments

This work is supported as part of the research project "Design of New Energy Materials" (No. 2021-12) by the State Commission of Science and Technology, DPR Korea. Computations were performed on the HP Blade System C7000 (HP BL460c) that is owned by Faculty of Materials Science, Kim Il Sung University.

References

(1) Bell, L. E. Cooling, Heating, Generating Power, and Recovering Waste Heat with Thermoelectric Systems, *Science* **2008**, *321*, 1457–1461.

(2) Zhao, L. D.; Tan, G.; Hao, S.; He, J.; Pei, Y.; Chi, H.; Wang, H.; Gong, S.; Xu, H.; Dravid, V. P.; Uher, C.; Snyder, G. J.; Wolverton, C.; Kanatzidis, M. G. Ultrahigh Power Factor and Thermoelectric Performance in Hole-Doped Single-Crystal SnSe, *Science* **2016**, *351*, 141–144.

(3) Mukhopadhyay, S.; Reinecke, T. L. Lone-Pair Electron-Driven Thermoelectrics at Room Temperature, *J. Phys. Chem. Lett.* **2019**, *10*, 4117–4122.

(4) Liu, Y.; Shi, W.; Zhao, T.; Wang, D.; Shuai, Z. Boosting the Seebeck Coefficient for Organic Coordination Polymers: Role of Doping-Induced Polaron Band Formation, *J. Phys. Chem. Lett.* **2019**, *10*, 2493–2499.

(5) Wang, Q.; Yang, L.; Zhou, S.; Ye, X.; Wang, Z.; Zhu, W.; McCluskey, M. D.; Gu, Y. Phase-Defined van der Waals Schottky Junctions with Significantly Enhanced Thermoelectric Properties, *J. Phys. Chem. Lett.* **2017**, *8*, 2887–2894.

(6) Ziang, J.; Hangyu, W.; Xianghui, F.; Bing, X.; Yingchun, D.; Kai, W.; Yonghong, C. Superior Thermoelectric Performance of Ordered Double Transition Metal MXenes: $Cr_2TiC_2T_2$ (T = −OH or −F), *J. Phys. Chem. Lett.* **2019**, *10*, 5721–5728.

(7) Dong, L.; Ye, L.; Zhao, D.; Tong, L.; Gao, F.; Li, W.; Lu, P.; Bu, X.-H. Thermal Transport Engineering in Hybrid Organic-Inorganic Perovskite Phononic Crystals, *J. Phys. Chem. Lett.* **2020**, *11*, 5728–5733.

(8) Feng, Q.; Mingyu, H.; Jue, G.; Chunyu, G.; Yunzuen, Z.; Jun, G.; Min, C.; Zhenhua, G.; Nitin, P.; Yuanyuan, Z.; Jing, F. Enhanced Thermoelectric Performance in Lead-Free Inorganic $CsSn_{1-x}Ge_xI_3$ Perovskite Semiconductors, *J. Phys. Chem. C* **2020**, *124*, 11749–11753.

(9) Liu, T.; Zhao, X.; Li, J.; Liu, Z.; Liscio, F.; Milita, S.; Schroeder, B. C.; Fenwick, O. Enhanced Control of Self-Doping in Halide Perovskites for Improved Thermoelectric Performance, *Nat. Commun.* **2019**, *10*, 5750.

(10) Jong, U.-G.; Yu, C.-J.; Kye, Y.-H.; Hong, S.-N.; Kim, H.-G. Manifestation of the Thermoelectric Properties in Ge-Based Halide Perovskites, *Phys. Rev. Mater.* **2020**, *4*, 075403.

(11) Xie, H.; Hao, S.; Bao, J.; Slade, T. J.; Snyder, G. J.; Wolverton, C.; Kanatzidis, M. G. All-Inorganic Halide Perovskites as Potential Thermoelectric Materials: Dynamic Cation Off-Centering Induces Ultralow Thermal Conductivity, *J. Am. Chem. Soc.* **2020**, *142*, 9553–9563.

(12) Lee, W.; Li, H.; Wong, A. B.; Zhang, D.; Lai, M.; Yu, Y.; Kong, Q.; Lin, E.; Urban, J. J.; Grossman, J. C.; Yang, P. Ultralow Thermal Conductivity in All-Inorganic Halide Perovskites, *Proc. Natl. Acad. Sci. USA* **2017**, *114*, 8693–8697.

(13) Pisoni, A.; Jacimovic, J.; Barisic, O. S.; Spina, M.; Gaal, R.; Forro, L.; Horvath, E. Ultra-Low Thermal Conductivity in Organic-Inorganic Hybrid Perovskite $CH_3NH_3PbI_3$, *J. Phys. Chem. Lett.* **2014**, *5*, 2488–2492.

(14) Yang, R. X.; Skelton, J. M.; da Silva, E. L.; Frost, J. M.; Walsh, A. Spontaneous Octahedral Tilting in The Cubic Inorganic Cesium Halide Perovskites $CsSnX_3$ and $CsPbX_3$ (X = F, Cl, Br, I), *J. Phys. Chem. Lett.* **2017**, *8*, 4720–4726.

(15) Whalley, L. D.; Skelton, J. M.; Frost, J. M.; Walsh, A. Phonon Anharmonicity, Lifetimes, and Thermal Transport in $CH_3NH_3PbI_3$ from Many-Body Perturbation Theory, *Phys. Rev. B* **2016**, *94*, 220301(R).

(16) Zhao, D.; Skelton, J. M.; Hu, H.; La-o-vorakiat, C.; Zhu, J.-X.; Marcus, R. A.; Michel-Beyerle, M.-E.; Lam, Y. M.; Walsh, A.; Chia, E. E. M. Low-Frequency Optical Phonon Modes and Carrier Mobility in The Halide Perovskite $CH_3NH_3PbBr_3$ Using Terahertz Time-Domain Spectroscopy, *Appl. Phys. Lett.* **2017**, *111*, 201903.

(17) Jong, U.-G.; Yu, C.-J.; Kye, Y.-H.; Choe, S.-H.; Kim, J.-S.; Choe, Y.-G. Anharmonic Phonons and Phase Transitions in the Vacancy-Ordered Double Perovskite Cs_2SnI_6 from First-Principles Predictions, *Phys. Rev. B* **2019**, *99*, 184105.

(18) Shi, L.; Bucknall, M. P.; Young, L.; ahd L. Hu, M. Z.; Bing, J.; Lee, D. S.; Kim, J.; Wu, T.; Takamure, N.; Mckenzle, D. R.; Huang, S.; Green, M. A.; Ho-Baillie, A. W. Y. Gas Chromatography-Mass Spectrometry Analyses of Encapsulated Stable Perovskite Solar Cells, *Science* **2020**, *368*, eaba2412.

(19) Dong, Q.; Fang, Y.; Shao, Y.; Mulligan, P.; Qiu, J.; Cao, L.; Huang, J. Electron-Hole Diffusion Lengths >175 μm in Solution-Grown $CH_3NH_3PbI_3$ Single Crystals, *Science* **2015**, *347*, 967–970.

(20) Wang, L.; McCleese, C.; Kovalsky, A.; Zhao, Y.; Burda, C. Femtosecond Time-Resolved

Transient Absorption Spectroscopy of $CH_3NH_3PbI_3$ Perovskite Films: Evidence for Passivation Effect of PbI_2, *J. Am. Chem. Soc.* **2014**, *136*, 12205–12208.

(21) Kye, Y.-H.; Yu, C.-J.; Jong, U.-G.; Chen, Y.; Walsh, A. Critical Role of Water in Defect Aggregation and Chemical Degradation of Perovskite Solar Cells, *J. Phys. Chem. Lett* **2018**, *9*, 2196–2201.

(22) Stoumpos, C. C.; Malliakas, C. D.; Kanatzidis, M. G. Semiconducting Tin and Lead Iodide Perovskites with Organic Cations: Phase Transitions, High Mobilities, and Near-Infrared Photoluminescent Properties, *Inorg. Chem.* **2013**, *52*, 9019–9038.

(23) Wolf, S. D.; Holovsky, J.; Moon, S. J.; Loper, P.; Niesen, B.; Ledinsky, M.; Haug, F. J.; Yum, J. H.; Ballif, C. Organometallic Halide Perovskites: Sharp Optical Absorption Edge and Its Relation to Photovoltaic Performance, *J. Phys. Chem. Lett.* **2014**, *5*, 1035–1039.

(24) Davis, N. J. L. K.; de la Peńa, F. J.; Tabachnyk, M.; Richter, J. M.; Lamboll, R. D.; Booker, E. P.; Rivarola, F. W. R.; Griffiths, J. T.; Ducati, C.; Menke, S. M.; Deschler, F.; Greenham, N. C. Photon Reabsorption in Mixed $CsPbCl_3$:$CsPbI_3$ Perovskite Nanocrystal Films for Light-Emitting Diodes, *J. Phys. Chem. C* **2017**, *121*, 3790–3796.

(25) Chatterjee, S.; Pal, A. J. Influence of Metal Substitution on Hybrid Halide Perovskites: Towards Lead-free Perovskite Solar Cells, *J. Mater. Chem. A* **2018**, *6*, 3793–3823.

(26) Hata, T.; Giorgi, G.; Yamashita, K. The Effects of the Organic-Inorganic Interactions on the Thermal Transport Properties of $CH_3NH_3PbI_3$, *Nano Lett.* **2016**, *16*, 2749–2753.

(27) Yue, S.-Y.; Zhang, X.; Qin, G.; Hu, J. Y. M. Insight into the Collective Vibrational Modes Driving Ultralow Thermal Conductivity of Perovskite Solar Cells, *Phys. Rev. B* **2016**, *94*, 115427.

(28) Qian, X.; X, X. G.; Yang, R. Lattice Thermal Conductivity of Organic-Inorganic Hybrid Perovskite $CH_3NH_3PbI_3$, *Appl. Phys. Lett.* **2016**, *108*, 063902.

(29) Yu, C.-J. Advances in Modelling and Simulation of Halide Perovskites for Solar Cell Applications, *J. Phys. Energy* **2019**, *1*, 022001.

(30) Klarbring, J.; Hellman, O.; Abrikosov, I. A.; Simak, S. I. Anharmonicity and Ultralow Thermal Conductivity in Lead-Free Halide Double Perovskites, *Phys. Rev. Lett.* **2020**, *125*, 045701.

(31) Jong, U.-G.; Yu, C.-J.; Kye, Y.-H. Computational Prediction of Structural, Electronic, and Optical Properties and Phase Stability of Double Perovskites K_2SnX_6 (X = I, Br, Cl), *RSC Adv.* **2020**, *10*, 201.

(32) Maughan, A. E.; Ganose, A. M.; Candia, A. M.; Granger, J. T.; Scanlon, D. O.; Neilson, J. R. Anharmonicity and Octahedral Tilting in Hybrid Vacancy-Ordered Double Perovskites, *Chem. Mater.* **2018**, *30*, 472–483.

(33) Cai, Y.; Xie, W.; Chen, H. D. Y.; Thirumal, K.; Wong, L. H.; Mathews, N.; Mhaisalkar, S. G.; Sherburne, M.; Asta, M. Computational Study of Halide Perovskite-Derived A_2BX_6 Inorganic Compounds: Chemical Trends in Electronic Structure and Structural Stability, *Chem. Mater.* **2017**, *29*, 7740–7749.

(34) Momma, K.; Izumi, F. VESTA 3 for Three-Dimensional Visualization of Crystal, Volumetric and Morphology Data, *J. Appl. Crystallogr.* **2011**, *44*, 1272–1276.

(35) *Crystallographic Database*. `http://crystallography.net/cod/4117957.html`.

(36) *Crystallographic Database*. `http://crystallography.net/cod/1010053.html`.

(37) Maughan, A. E.; Ganose, A. M.; Bordelon, M. M.; Miller, E. M.; Scanlon, D. O.; Neilson, J. R. Defect Tolerance to Intolerance in the Vacancy-Ordered Double Perovskite Semiconductors Cs_2SnI_6 and Cs_2TeI_6, *J. Am. Chem. Soc.* **2016**, *138*, 8453–8464.

(38) Maughan, A. E.; Ganose, A. M.; Almaker, M. A.; Scanlon, D. O.; Neilson, J. R. Tolerance Factor and Cooperative Tilting Effects in Vacancy-Ordered Double Perovskite Halides, *Chem. Mater.* **2018**, *30*, 3909–3919.

(39) Deng, Z.; Wei, F.; Sun, S.; Kieslich, G.; Cheetham, A. K.; Bristowe, P. D. Exploring the Properties of Lead-free Hybrid Double Perovskites Using a Combined Computational-Experimental Approach, *J. Mater. Chem. A* **2016**, *4*, 12025–12029.

(40) Patrick, C. E.; Jacobsen, K. W.; Thygesen, K. S. Anharmonic Stabilization and Band Gap Renormalization in the Perovskite $CsSnI_3$, *Phys. Rev. B* **2015**, *92*, 201205.

(41) *Crystallographic Database*. `http://crystallography.net/cod/4117958.html`.

(42) *Crystallographic Database*. `http://crystallography.net/cod/4117956.html`.

(43) Xia, Y.; Chan, M. K. Y. Anharmonic Stabilization and Lattice Heat Transport in Rocksalt β-GeTe, *Appl. Phys. Lett.* **2018**, *113*, 193902.

(44) Jong, U.-G.; Kim, Y.-S.; Ri, C.-H.; Kye, Y.-H.; Yu, C.-J. High Thermoelectric Performance in the Cubic Inorganic Cesium Iodide Perovskites $CsBI_3$ (B = Pb, Sn, and Ge) from First-Principles, *J. Phys. Chem. C* **2021**, *125*, 6013–6019.

(45) Tadano, T.; Gohda, Y.; Tsuneyuki, S. Anharmonic Force Constants Extracted from Frst-Principles Molecular Dynamics: Applications to Heat Transfer Simulations, *J. Phys.: Condens. Matter* **2014**, *26*, 225402.

(46) Tadano, T.; Tsuneyuki, S. Self-Consistent Phonon Calculations of Lattice Dynamical Properties in Cubic $SrTiO_3$ with First-Principles Anharmonic Force Constants, *Phys. Rev. B* **2015**, *92*, 054301.

(47) Qi, J.; Dong, B.; Zhang, Z.; Zhang, Z.; Chen, Y.; Zhang, Q.; Danilkin, S.; Chen, X.; He, J.; Fu, L.; Jiang, X.; Chai, G.; Hiroi, S.; Ohara, K.; Zhang, Z.; Ren, W.; Yang, T.; Zhou, J.;

Osami, S.; He, J.; Yu, D.; Li, B.; Zhang, Z. Dimer Rattling Mode Induced Low Thermal Conductivity in An Excellent Acoustic Conductor, *Nat. Commun.* **2020**, *11*, 5197.

(48) Fabini, D. H.; Laurita, G.; Bechtel, J. S.; Stoumpos, C. C.; Evans, H. A.; Kontos, A. G.; Raptis, Y. S.; Falaras, P.; Van der Ven, A.; Kanatzidis, M. S.; Seshadri, R. Dynamic Stereochemical Activity of the Sn(2+) Lone Pair in Perovskite $CsSnBr_3$, *J. Am. Chem. Soc.* **2016**, *138*, 11820–11832.

(49) Snyder, G. J.; Toberer, E. S. Complex Thermoelectric Materials, *Nat. Mater.* **2008**, *7*, 105–114.

(50) Xia, Y.; Pal, K.; He, J.; Ozolins, V.; Wolverton, C. Particlelike Phonon Propagation Dominates Ultralow Lattice Thermal Conductivity in Crystalline Tl_3VSe_4, *Phys. Rev. Lett.* **2020**, *124*, 065901.

(51) He, J.; Hao, S.; Xia, Y.; Naghavi, S. S.; Ozolins, V.; Wolverton, C. Bi_2PdO_4: A Promising Thermoelectric Oxide with High Power Factor and Low Lattice Thermal Conductivity, *Chem. Mater.* **2017**, *29*, 2529–2534.

(52) Blöchl, P. E. Projector Augmented-Wave Method, *Phys. Rev. B* **1994**, *50*, 17953–17979.

(53) Kresse, G.; Furthmüller, J. Effciency of Ab-Initio Total Energy Calculations for Metals and Semiconductors Using a Plane-Wave Basis Set, *Comput. Mater. Sci.* **1996**, *6*, 15–50.

(54) Kresse, G.; Furthmüller, J. Efficient Iterative Schemes for Ab Initio Total-Energy Calculations Using a Plane-Wave Basis Set, *Phys. Rev. B* **1996**, *54*, 11169–11186.

(55) Perdew, J. P.; Ruzsinszky, A.; Csonka, G. I.; Vydrov, O. A.; Scuseria, G. E.; Constantin, L. A.; Zhou, X.; Burke, K. Restoring the Density Gradient Expansion for Exchange in Solids and Surfaces, *Phys. Rev. Lett.* **2008**, *100*, 136406.

(56) Zhou, F.; Nielson, W.; Xia, Y.; Ozolins, V. Lattice Anharmonicity and Thermal Conductivity from Compressive Sensing of First-Principles Calculations, *Phys. Rev. Lett.* **2014**, *113*, 185501.